18TH WORLD CONFERENCE ON EARTHQUAKE ENGINEERING
WCEE2024
MILAN

MILAN, ITALY
30TH JUNE - 5TH JULY 2024

www.wcee2024.it

SEISMIC BEHAVIOR OF ISOLATED STRUCTURES UNDER SUBDUCTION AND CRUSTAL GROUND MOTIONS: A COMPARATIVE STUDY

F. Gutiérrez-Urzúa[1], F. Freddi[1], J.C. de la Llera[2,3], J.G.F. Crempien[2,3], J.A. Gallardo[2,3], J.P. Muñoz[3], T. Rossetto[1], S. Dede[1], J. Cembrano[2], F. Rivera[1], & M.F. Chacón[3,4]

[1] Dept. Civil, Env. & Geomatic Engineering, University College London, London, UK, f.urzua@ucl.ac.uk

[2] Dept of Structural and Geotechnical Engineering, Pontificia Universidad Católica de Chile, Santiago, Chile

[3] Research Center for Integrated Disaster Risk Management (CIGIDEN), Santiago, Chile

[4] Centro Nacional de Excelencia para la Industria de la Madera (CENAMAD), Pontificia Universidad Católica de Chile, Santiago, Chile

Abstract: *Seismic isolation decouples the modal characteristics of the structure from those of the ground motion, thus reducing structural demands, particularly under intense earthquakes. Seismic isolation is particularly beneficial when used for strategic facilities such as hospitals, as it often allows the building to remain operational in the aftermath of an earthquake-related disaster. Although the use of these devices is widespread in earthquake-prone regions, there are still open issues that require to be studied. These open issues include the performance and reliability of the seismic isolation systems when subjected to earthquakes with characteristics that are different than those considered during the design. The present study investigates the seismic performance of a case study isolated hospital with a high-damping rubber compound in Santiago, Chile, considering sets of ground motions generated by either megathrust subduction or crustal fault mechanisms. A 3D finite element model of a case study hospital is developed in OpenSees. Sets crustal ground motions resulting from earthquake rupture scenarios on the San Ramon Fault are generated by the UCSB method, which involves simulating a synthetic earthquake source with specified temporal and spatial slip on the fault. Successively, sets of 'equivalent' recorded subduction ground motions are selected. Incremental Dynamic Analyses (IDAs) are used to compute different local and global Engineering Demand Parameters (EDPs) considering records from the two types of events (subduction vs. crustal), both considering and not considering the vertical component of the ground motion. The results show the paramount importance of considering different seismic sources to better understand/predict the seismic response of isolated structures.*

1. Introduction

The subduction zone between the Nazca and South American plates, capable of generating megathrust earthquake events, strongly governs the seismicity of Chile. Some of the largest magnitude historical earthquake events have been registered in that region, including the M_w = 9.5 1960 Valdivia Earthquake, the M_w = 8.8 2010 Maule Earthquake, and the M_w = 8.2 1906 Valparaíso earthquake (Ruiz S and Madariaga, 2018). The 1960 Valdivia Earthquake was the largest magnitude earthquake ever recorded. The epicentre was located near Lumaco, approximately 570 km south of Santiago, with an estimated rupture length of over 1,000 km, being Valdivia the most affected city. The economic losses are estimated to lie between four and

eight billion USD (adjusted to 2022 for inflation), while thousands of casualties were documented. The 2010 Maule Earthquake occurred off the coast of Central Chile in February 2010, with a recorded intense shaking of around three minutes. It was perceived as strong in six Chilean regions (from Valparaíso to Araucanía), which comprise 80% of the country's population. Official sources stated that about 9% of the population in the affected regions lost their homes. The estimated total losses are estimated between $15 to $30 billion USD. The 1906 Valparaíso Earthquake was a result of a 400 km long rupture on the tectonic plate boundary, which resulted in widespread destruction and damage throughout Central Chile, from Illapel to Talca. This kind of subduction megathrust events have influenced the development of national design standards (INN 1996, INN 2013), and have pushed Chilean structural design towards non-conventional solutions to improve the seismic-resiliency and operativity of strategic infrastructure in the aftermath of a strong earthquake (de la Llera *et al.* 2015; de la Llera *et al.* 2017; Simpson *et al.* 2018, Freddi *et al.* 2021).

Some of these solutions involve the use of seismic isolation systems, which allow minimising the structural and non-structural damage and allow the building to remain operational after a seismic event. This is particularly relevant for buildings that are essential in the disaster response, such as hospitals. In fact, several studies have demonstrated that base-isolation is highly effective in protecting new and existing structures from earthquake demands from the subduction region. Many of the most recent applications involve the use of Lead Rubber Bearings (LRBs) or High Damping Rubber Bearings (HDRBs) along with Low-Friction Sliding Bearings (LFSDs), which allow achieving long fundamental periods on the superstructure while simultaneously allowing the control of the eccentricities that would result on global torsional effects and excessive deformation demands on the corner and edge isolators. Moreover, the isolation system significantly reduces the demands transferred to the superstructure, which improves the performance of the building in both service and ultimate limit states (de la Llera *et al.* 2004). Yet, most of these structures have been designed by considering the earthquake hazard from the subduction region, while the intraplate seismicity is often overlooked.

Nonetheless, considerable efforts have been made to characterise the seismicity of intraplate crustal faults that are a potential seismic threat to the region, particularly to Santiago. One example of this is the San Ramon Fault (SRF), a 35 km crustal fault that lies on the Eastern edge of the urban footprint of Santiago in a North-South direction (-70°30' longitude), and dips to the east on an angle of about 55° (Diaz *et al.* 2014). This fault is considered potentially active (Armijo *et al.* 2010), yet the amount of energy that can be released in a single event is a matter of debate among seismologists; therefore, its potential impact on the city of Santiago is uncertain. Although the earthquake magnitudes from events originated by the SRF are not comparable to those of the subduction region, its proximity to the city of Santiago makes its study highly relevant.

To investigate this issue, the present paper compares the seismic performance of a real case study isolated hospital equipped with HDRBs and LFSBs in Santiago (Figure 1), considering sets of two and three-dimensional ground motions generated by either the megathrust subduction region or the SRF.

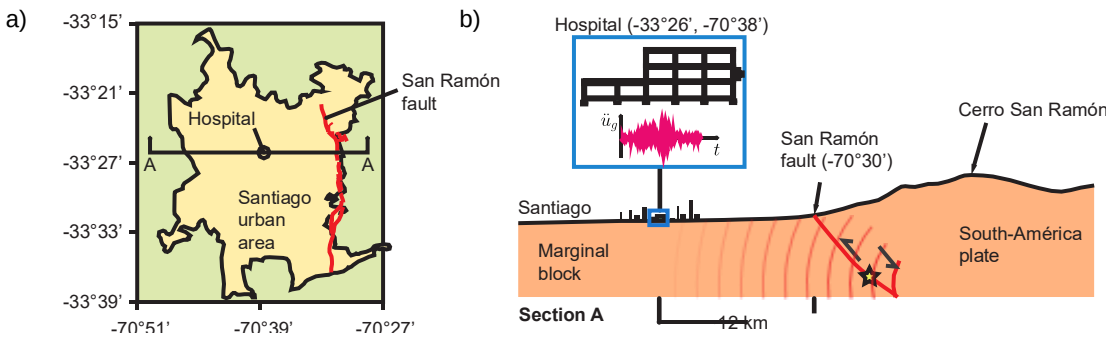

Figure 1. (a) Plan view of the Metropolitan region; and (b) schematic cross-section East-West, including a schematic representation of the San Ramon Fault.

For this purpose, a set of 3-dimensional crustal synthetic ground motions is generated using the UCSB method (Crempien and Archuleta 2017), simulating synthetic earthquakes originated by the SRF, with specified temporal and spatial slip on the fault. In particular, this simulation assumes a moment magnitude M_w = 6.5, a corner frequency of the moment-rate spectra f_c = 0.14 Hz, and an average rupture velocity V_r = 3.0 km/s. These assumptions are considered representative of a potential earthquake scenario at the SRF. In addition,

a set of 3-dimensional 'equivalent' subduction ground motion records are selected to match the spectral mean and dispersion in the logarithmic scale. A total of 16 multi-dimensional records are considered for each of the 2 sets. A detailed 3-dimensional model of the case study hospital is developed in OpenSees (McKenna *et al.* 2000), including detailed modelling of the seismic isolation system. The numerical model is subjected to the ground motion records on each set through non-linear time-history analyses to investigate the structure's seismic response. Relevant local and global Engineering Demand Parameters (EDPs) are considered and compared to design capacity limits. This study highlights the importance of considering nearby seismic sources to better understand the performance of the structure, particularly when the design was carried out without considering them.

2. Case Studies Structure & Finite Element (FE) Modelling

1.1. Case Study Structure

The chosen hospital for this case study is situated in downtown Santiago and underwent significant renovation between 2013 and 2014. The revamped structure consists of two adjacent reinforced concrete (RC) moment-resisting frame buildings. The primary building, central to this research, boasts a subsurface portion with two basements featuring robust retaining shear walls along the perimeter. Its superstructure comprises three stories, characterized by a regular orthogonal grid of moment-resisting frames spaced 8.00 meters apart. The isolation level is positioned at the junction of the substructure and superstructure and encompasses 33 HDRBs (High-Damping Rubber Bearings) and 19 LFSBs (Lead Rubber Bearings). The structure is located in seismic Zone 2 with soil type 2 (very stiff gravel) (INN 2013). Concrete of grade C25 with compressive strength f'_c = 25 MPa and A630-420H grade steel bars with a yield stress f_y = 420 MPa were employed in the design. Figure 2 illustrates the structure's layout plan and elevation view, highlighting the placement of various isolator devices and providing details on the HDRBs utilized in the design. The seismic isolation system was devised in accordance with the NCh2745 code design spectrum, representing events with a 10% exceedance probability over 50 years (PGA = 0.4g). Furthermore, the stability of the devices was validated for maximum earthquakes with a 10% exceedance probability over 100 years (PGA = 0.48g).

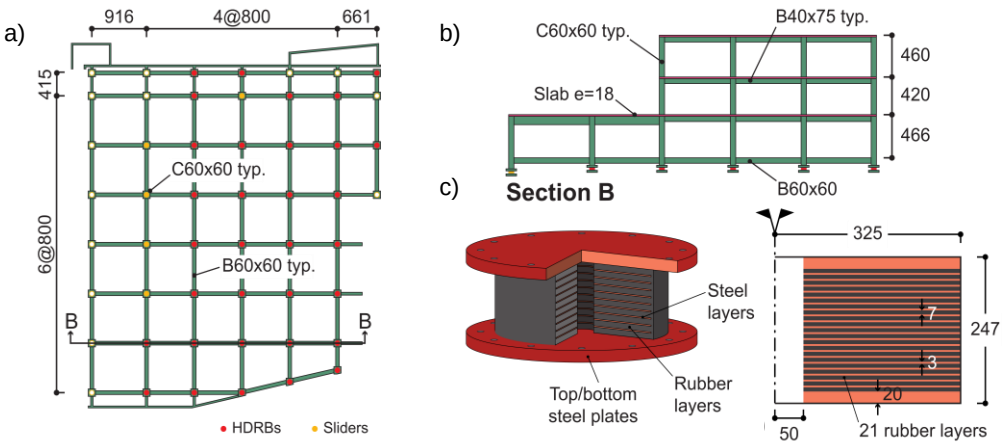

Figure 2. Case-study hospital building: (a) plan view of the isolation system; (b) typical elevation of the isolated structure; and (c) scheme of the HDRBs.

The 33 HDRBs have external and internal diameters of 650 mm and 100 mm, respectively, a height of 247mm, and are characterised by nominal elastomer shear modulus G = 3.924 MPa. The design and the maximum total displacements for the isolators are 239 mm and 249 mm, respectively. Also, the design limits for the short-term axial forces in the HDRBs were assumed as 1.18 MPa in tension and 22.56 MPa in compression. At the design displacement, the damping ratio of the rubber must be larger than 9%, and the horizontal stiffness must be within the range between 764.92 kN/m and 1029.70 kN/m. On the other end, the 19 LFSBs have diameters of 350 and 450 mm, and are characterised by a nominal friction coefficient between 5-7% for velocities exceeding 150 mm/s. The maximum axial stresses for the sliders are 15 MPa and 22 MPa, respectively, for long- and short-term loads.

1.2. Finite Element (FE) Modelling

Figure 3 shows the 3D FE model of the case study structure that was developed in OpenSees to conduct time-history analyses under the two sets of GM records. The modelling focused only on the superstructure. Modelling of the substructure was neglected as preliminary analyses revealed that, as a consequence of the large stiffness provided by the retaining shear walls, the contribution of the substructure to the dynamic response of the whole building is negligible. Additionally, to reduce the computational efforts required by the analyses, beams and columns in the superstructure (*i.e.*, structural elements above the isolation layer) are assumed to behave elastically and thus modelled as '*elasticBeamColumn'* elements (E_c = 23,500 MPa). This assumption is sustained as these elements were confirmed not to overpass their yielding capacity. A '*rigidDiaphragm'* constraint is included on the nodes at each floor level to represent the diaphragm effect provided by the RC slabs, including the floor above the isolation layer. The gravity load and the seismic mass used for the non-linear time-history analysis correspond to the self-weight plus 25% of the live loads according to the Chilean code (INN 1996) and were uniformly distributed on the slabs at each floor.

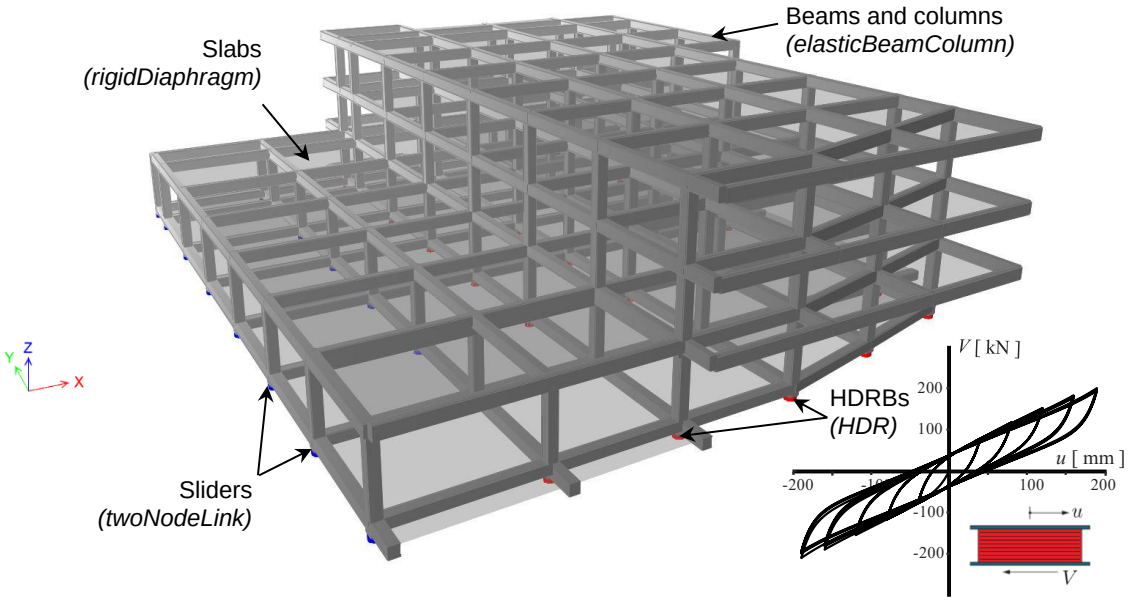

Figure 3. Case-study building: (a) 3D view of the FE model, and (b) shear force-lateral displacement hysteresis of the HDRB model.

The HDRBs were modelled using the 2-node '*HDR'* bearing element in OpenSees, which uses the model proposed by Grant *et al.* (2004) for simulating the shear response, and by Kumar *et al.* (2014) for cavitation under tensile loads. Linear and uncoupled responses were assumed for the axial response and the other three rotational degrees of freedom. Similarly, the LFSBs were modelled by the '*twoNodeLink*' element with the uniaxial '*Elastic*' material in both directions, as it is assumed that their shear stiffness remains largely constant within the drift values considered in this study. A Rayleigh damping model was used for the damping matrix of the superstructure, with a critical damping ratio of 2% for the first two natural vibration modes. This damping only applies to the superstructure as the isolation layer's energy dissipation is explicitly modelled.

3. Ground Motions (GMs) generation and selection

This section describes the generation of the crustal GMs and the selection of subduction GMs records used for the non-linear time-history analyses of the case-study structure.

1.3. Crustal ground motion (GM) records

Crustal GMs originated by the rupture of the SRF have been generated by the UCSB method (Liu *et al.* 2006; Schmedes *et al.* 2013; Crempien and Archuleta 2015; Crempien and Archuleta 2017). This is done by simulating a synthetic earthquake source with specified temporal and spatial slip on the fault. To propagate waves away from the fault, the procedure relies on the discrete wavenumber technique proposed by Zhu and Rivera (2002), which computes appropriate Green's functions based on a 1D layered velocity structure. The

moment magnitude (M_w), the corner frequency of the moment-rate spectra (f_c), and the average rupture velocity (V_r) were assumed equal to 6.5, 0.14 Hz, and 3.0 km/sec, respectively. The corner frequency was forced to have a value consistent with the scaling of this parameter with the magnitude, as proposed by Aki (1967), while the rupture velocity was assumed to be independent. The spatial characteristics of final slip, rise-time, peak-time, and rupture velocity on the fault were prescribed based on a von Kármán power spectrum correlation structure, with the parameters proposed by Crempien & Archuleta (2015) guiding the correlation structure of the rupture parameters. The fault dimensions were scaled using the relationship proposed by Leonard (2010), which yields a length of 20 km, and a width of 10 km, for the considered M_w 6.5 earthquakes. To account for uncertainties in the GM and by utilising the simulated earthquake source parameters, a total of 16 GM rupture scenarios were produced and computed at the specific location of the case study hospital.

1.4. Subduction ground motion (GM) records

Subduction GMs have been selected to be 'equivalent' to the crustal records in terms of the response spectra of their horizontal components. The selection procedure is summarised by the following steps:

1. The maximum direction response spectrum (RotD100) is computed for each crustal GM, considering a damping ratio of ξ = 5% and 50 vibrations periods distributed uniformly (in logarithmic scale) between 0.01 s and 5.00 s;
2. The mean (in logarithm scale) RotD100 spectrum is computed for the crustal records response spectra at each vibration period;
3. An initial pool of candidate GMs is obtained from the SIBER-RISK seismic database[1], and their RotD100 response spectra are computed;
4. A scaling factor $\alpha^{s,k}$ is computed for each candidate subduction record as shown in the following Eq. (1):

$$\alpha^{s,k} = \frac{\sum_{j=1}^{n} S_a^{c,\mu}(T_j)}{\sum_{j=1}^{n} S_a^{s,k}(T_j)} \tag{1}$$

where $S_a^{c,\mu}$ is the mean RotD100 response spectrum of the crustal records, $S_a^{s,k}$ is the RotD100 response spectrum of the k-th subduction candidate GM and T_j's are the periods in the range of interest. Under this condition, only candidate GMs that required a scaling factor between 0.25 and 4.0 were initially considered;

5. One subduction record is selected for each crustal one by computing the sum of squared errors (SSE) between a scaled candidate subduction GM ($\alpha^{s,k}\, S_a^{s,k}$) and the target crustal GM ($S_a^{c,i}$), in the range of periods of interest (T_j), as shown in the following Eq. (2):

$$SSE_{i,k} = \sum_{j=1}^{n} \left(\ln\left(S_a^{c,i}(T_j)\right) - \ln\left(\alpha^{s,k}\, S_a^{s,k}(T_j)\right) \right)^2 \tag{2}$$

6. The candidate record with the lowest SSE value is then selected.

By following this approach, the set of selected subduction records closely matches the crustal GMs set in terms of the mean and variance of the RotD100 response spectra. It is worth mentioning that the vertical component is not considered in the selection process but is instead selected as an afterthought and scaled by the same factor used for the horizontal components.

Figure 4 shows the comparison between the response spectra of the set of records for the crustal and subduction GMs in red and black lines, respectively. Bold solid lines represent the mean spectra of the natural logarithm of the accelerations, while the bold dotted lines represent the mean spectra ± one standard deviation. The figure shows how the two sets of records are comparable in terms of horizontal spectral accelerations.

[1] https://www.siberrisk.cl/

4. Dynamic Response and Performance Assessment

Figure 5 shows and reports the natural vibration modes and fundamental periods of the isolated structure. The first two vibration modes are, respectively, in the X- and Y-directions and have long and almost identical lateral vibration periods (*i.e.,* T_1 = 2.849 sec and T_2 = 2.845 sec) due to the presence of the isolation system. The third mode of vibration is torsional and also has a long period but slightly stiffer (*i.e.,* T_3 = 2.719 sec). The higher natural vibration modes are translational (*i.e.,* Mode 4 and 5) and torsional (*i.e.,* Mode 6) and are characterised by similar vibration periods.

The time-history analyses are carried out by considering the two sets of 16 GM triplets, as detailed in previous sections. For the crustal GMs, the two horizontal components were applied, considering the real orientation of the case-study structure with respect to the seismic sources. Conversely, the subduction GMs records were applied considering the orientation of the records measured at the stations. The following part of the paper describes and compares the response of the structure under the two sets of GMs considering global and local EDPs of interest, *i.e.,* displacements, accelerations, displacements, and forces in the HDRBs.

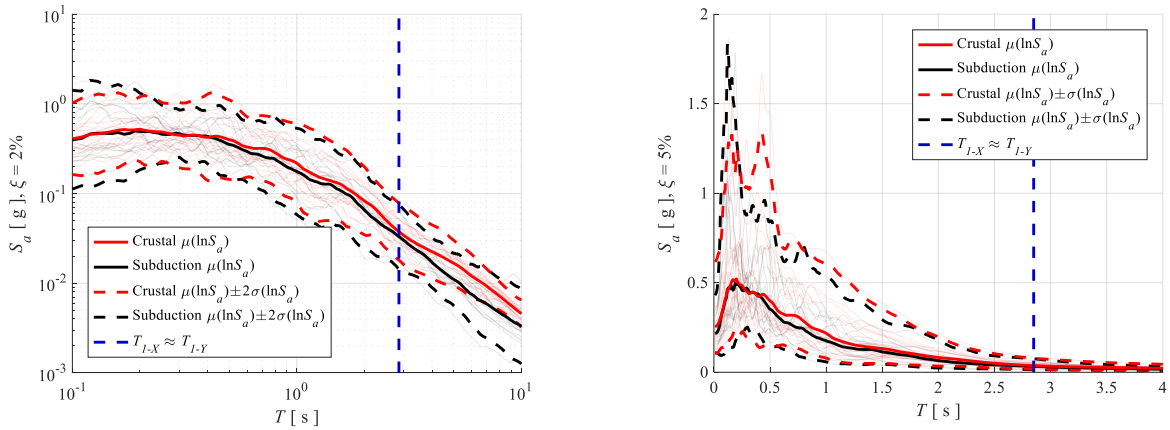

(a) Logarithmic space (b) Linear space

Figure 4. Comparison of the response spectra for the crustal and subduction GMs for horizontal components.

Figure 6 and Figure 7 show the response of the structure, respectively, in terms of displacements and accelerations in X- and Y-directions at the roof and isolation slab for the crustal and subduction GM records. These figures show the orbits for the time-history analyses together with the peak values. The results show minor differences in displacements for the roof and isolation slab, highlighting the effectiveness of the isolation system in limiting deformations of the superstructure (Figure 6). Some small differences can be observed in terms of accelerations, which are slightly amplified due to the response of the superstructure, *i.e.,* slightly higher accelerations at the roof with respect to the isolation slab (Figure 7). The comparison between the results of the two sets of GMs shows that the crustal GMs result in more significant displacement and acceleration demands. Moreover, the response of the structure under this set of records is affected by strong directionality effects. This is a consequence of the strong N-S component of the crustal GMs rather than a property of the building. It is worth reminding the readers that the fundamental periods of the isolated structure are almost identical in X- and Y-directions as a consequence of the isolators. Simulations of the subduction GM records have been carried out also considering them with a 90-degree rotation, and the results did not show any significant difference in terms of peak values of the considered global and local EDPs. These results are not shown here for the sake of brevity.

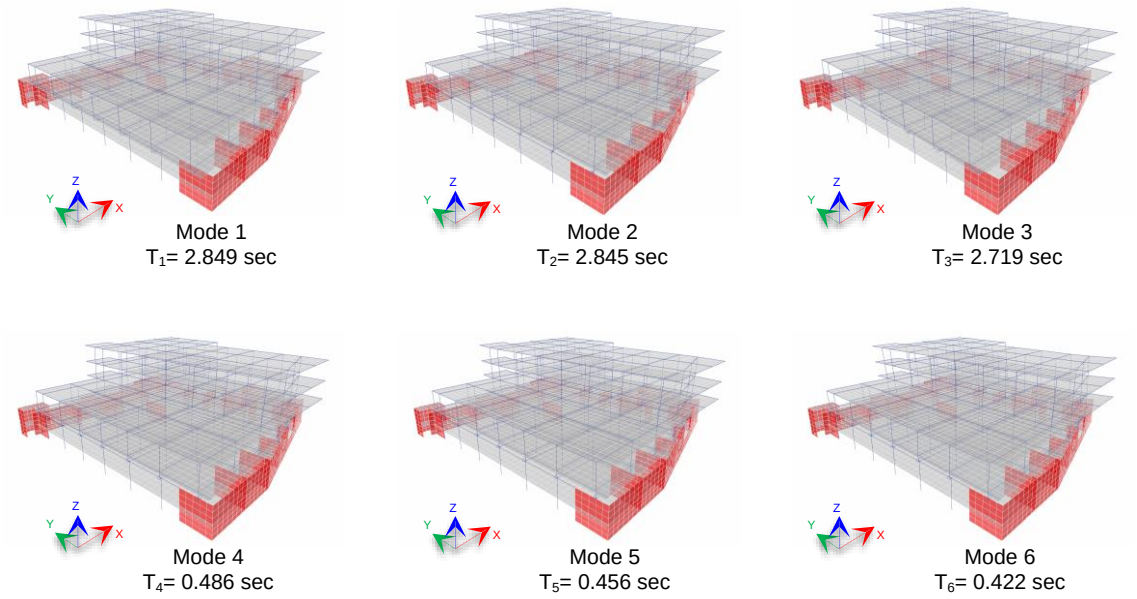

Figure 5. Mode-shapes and natural vibration periods.

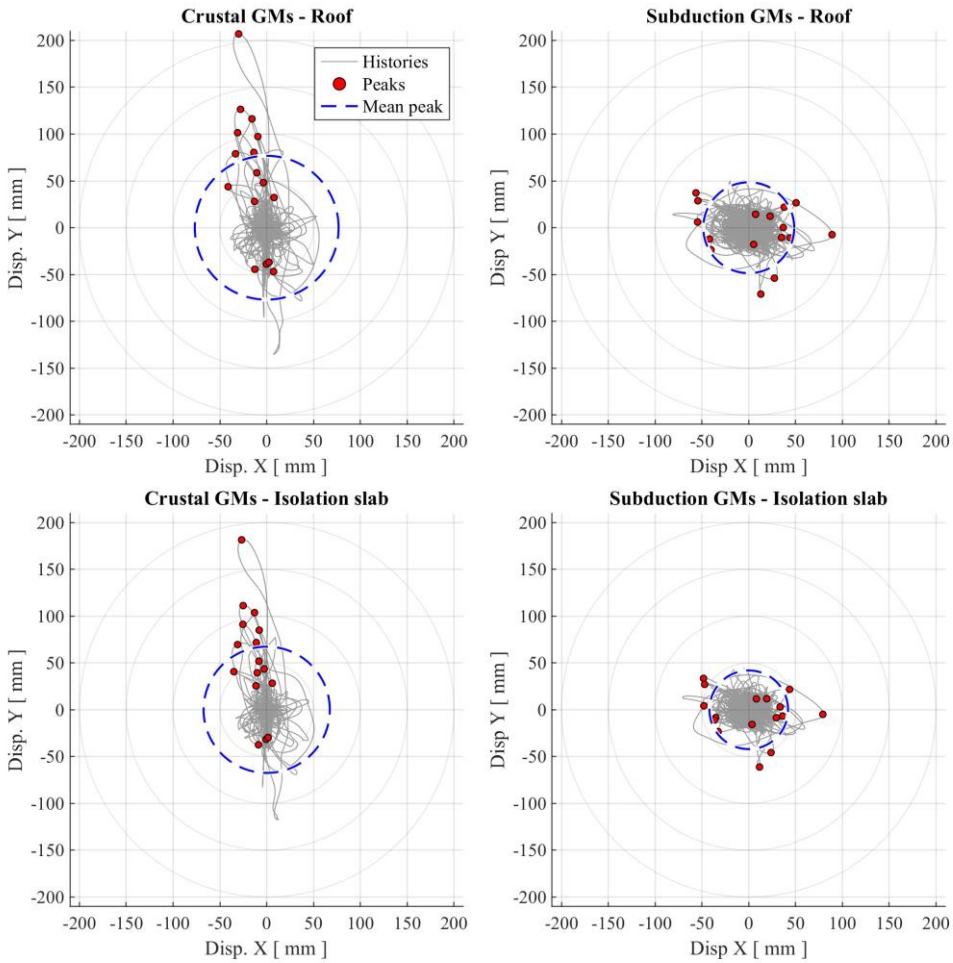

Figure 6. Comparison of displacement orbits for crustal and subduction GM records at the isolation slab and roof.

Figure 8 shows the local responses in terms of peak horizontal displacements of all isolators and for all records of the two sets of GMs. Consistently with the global responses, it can be observed that the crustal GMs result in larger horizontal displacements. The mean peak horizontal deformation imposed on the isolators (black dotted lines in Figure 8) during the crustal GMs is about 65 mm, contrasting with the approximately 45 mm observed in the subduction GMs. This figure also includes the maximum deformation capacity of the isolators (red dotted lines in Figure 8), showing that, despite the larger deformation demand experienced during crustal GMs, the isolators are still within the design limits. Figure 9 shows the local responses in terms of axial forces of all isolators and for all records of the two sets of GMs. Maximum and minimum demand values for crustal and subduction GMs are reported and compared with demand values deriving from gravity loads only. This figure also includes the design maximum (tension) and minimum (compression) axial force threshold values (*i.e.,* design limit states), corresponding to 382 kN and 7309 kN (red dotted lines in Figure 9). In this case, it is observed that the crustal GM records generate demand values, overcoming these limits for a few cases.

The figure also shows the mean values for these parameters (magenta and cyan lines in Figure 9), highlighting that the crustal GMs generate a much larger variability of the axial forces in the HDRBs compared with the subduction GM records. This effect is mainly due to the more significant vertical component of the crustal GMs compared with the subduction ones. This can be more easily observed by comparing Figure 9 to Figure 10, as the latter illustrates the demands when the vertical component of the ground motion is not included; thus, the differential between the gravity loading and the maximum and minimum axial loads is entirely attributed to the overturning effects resulting from the horizontal earthquake loading.

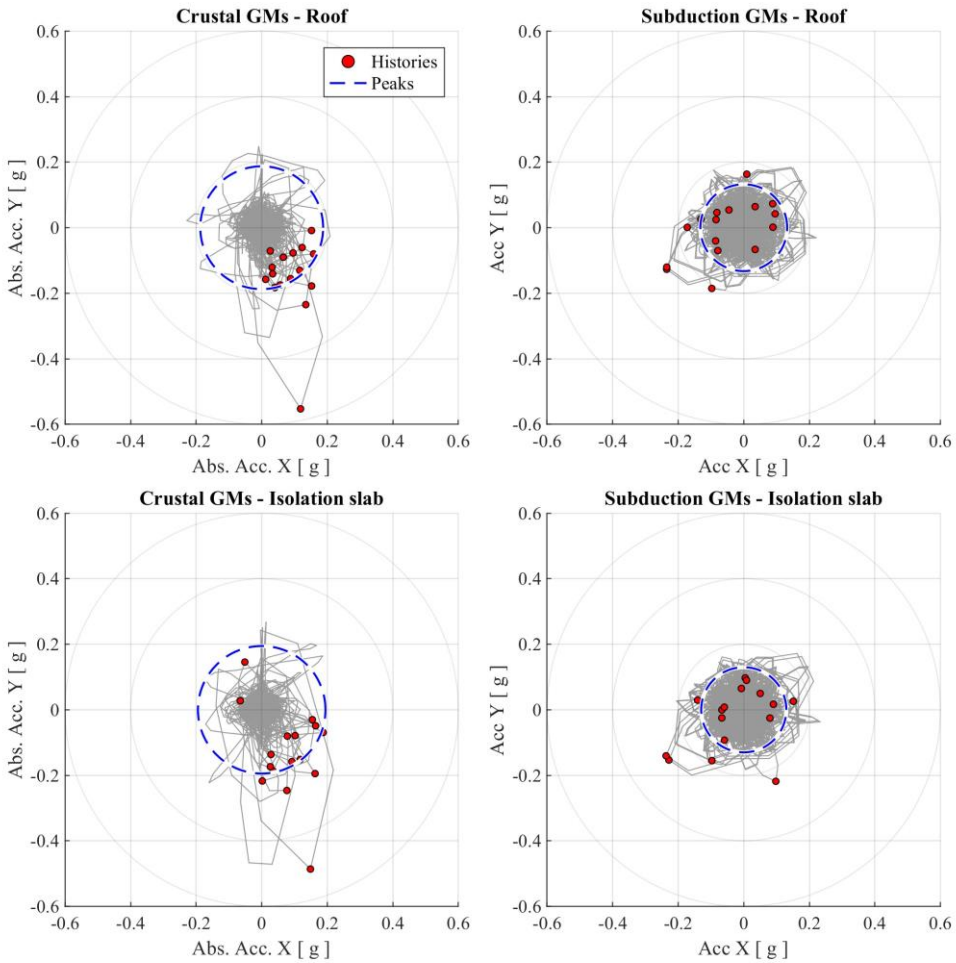

Figure 7. Comparison of acceleration orbits for crustal and subduction GM records at the isolation slab and roof.

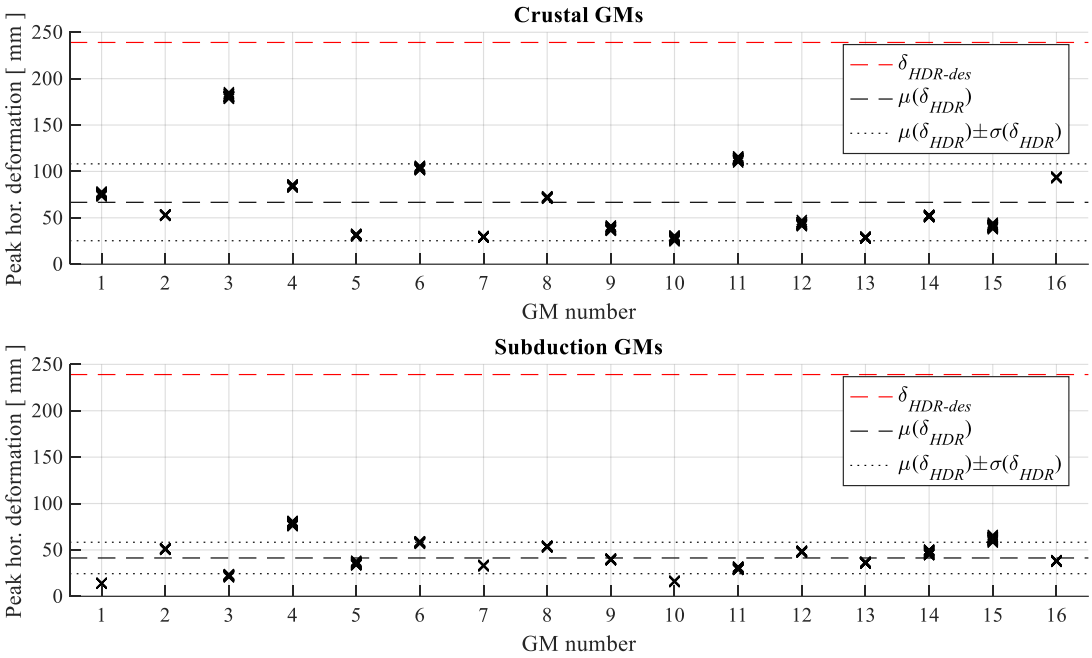

Figure 8. Peak horizontal deformations of HDRB isolators subjected to crustal and subduction GM records.

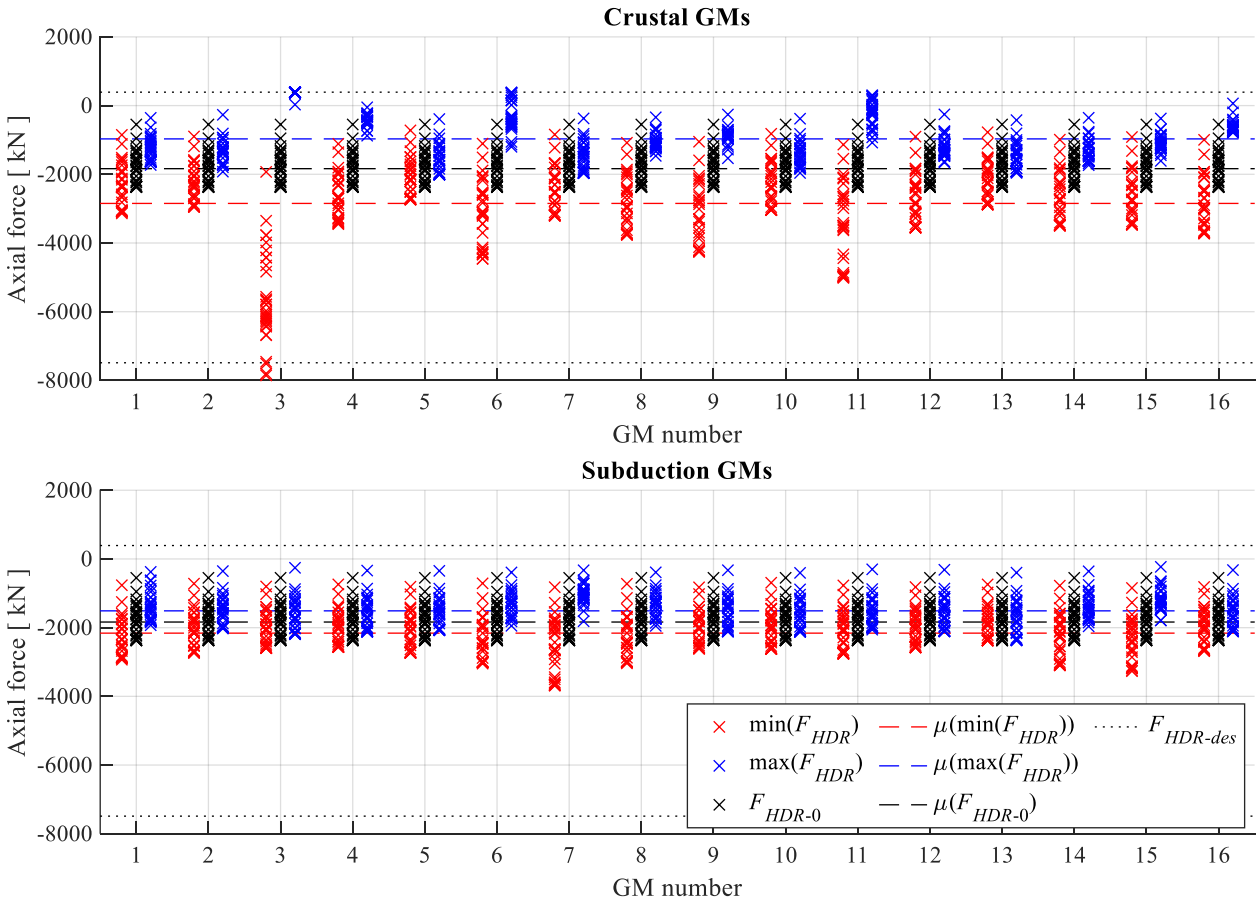

Figure 9. Axial loads imposed on HDRB isolators. Maximum and minimum demand values for crustal and subduction GM records when considering the vertical acceleration component, and demand values for gravity loads only.

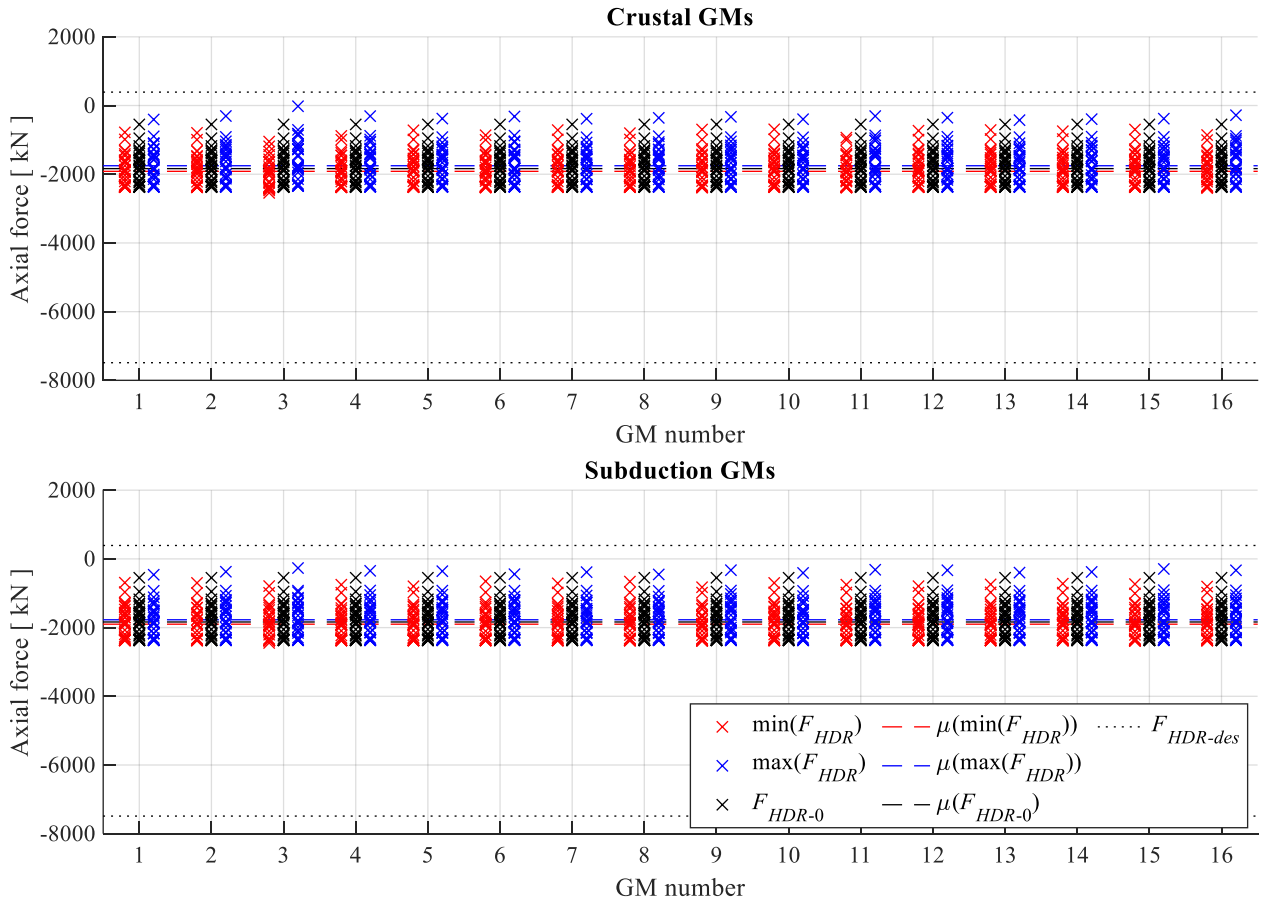

Figure 10. Axial loads imposed on HDRB isolators. Maximum and minimum demand values for crustal and subduction GM records when not considering the vertical acceleration component, and demand values for gravity loads only.

5. Conclusions

The present study compares the seismic response of a base-isolated hospital in Santiago, Chile, subjected to crustal and subduction earthquakes. The effectiveness of the seismic isolation system is evaluated by contrasting the response of the structure for each set of ground motion (GM) records and comparing the demands on the isolators to their design limits. The results show that the seismic isolation system is effective in limiting the demands on the superstructure, as the displacements along the height of the building are similar regardless of the GMs type. However, the response of the structure under crustal GMs results in larger displacement and acceleration demands compared to subduction GMs. Despite the larger deformation demand experienced during crustal GMs, the isolators were found within the design limits in all cases. Conversely, it is observed that the axial forces in the HDRBs vary much more with crustal GMs compared to subduction GMs due to the more significant vertical component of crustal GMs. The preliminary results show that, in very few cases, the crustal GM records generate demand values that slightly overcome the design limit states for axial force threshold values.

6. Acknowledgements

This research has been sponsored by FONDECYT, under the project ‘Multiscale earthquake risk mitigation of healthcare networks using seismic isolation’, ANID/ FONDECYT/ 1220292 and ANID/doctorate scholarship/21201370, the Research Center for Integrated Disaster Risk Management (CIGIDEN), ANID/ FONDAP/ 1522A0005; and the 2022 Seed Fund UCL-PUC research initiative. The authors are grateful for all the support.

7. References

Aki K. (1967). Scaling law of seismic spectrum. *Journal of Geophysical Research*, 72(4): 1217-1231.

Armijo R., Rauld R., Thiele R., Vargas G., Campos J., Lacassin R., Kausel E. (2010), The West Andean Thrust, the San Ramón Fault, and the seismic hazard for Santiago, Chile, *Tectonics*, 29: 1-34.

Crempien J., Archuleta R. (2015). UCSB Method for Simulation of Broadband Ground Motion from Kinematic Earthquake Sources. *Seismological Research Letters*, 86: 61–67.

Crempien J., Archuleta R. (2017). Within-Event and Between-Events Ground Motion Variability from Earthquake Rupture Scenarios. *Pure and Applied Geophysics*, 174: 3451–3465.

de la Llera J.C., Lüders C., Leigh P., Sady H. (2004). Analysis, testing, and implementation of seismic isolation of buildings in Chile. *Earthquake Engineering and Structural Dynamics*, 33(5): 543 – 574.

de la Llera J.C., Mitrani-Reiser J., Rivera J., Fortuño C., Jünemann R., Poulos A., Vásquez J. (2015). The 2010 Chile earthquake: a five year reflection, *Proceedings of the 10th Pacific Conference on Earthquake Engineering*, Sydney, Australia.

de la Llera J.C., Rivera F., Mitrani-Reiser J., Jünemann R., Fortuño C., Ríos M., Hube M., Santa María H., Cienfuegos R. (2017). Data collection after the 2010 Maule earthquake in Chile, *Bulletin of Earthquake Engineering*, 15(2): 555 – 5881

Díaz D., Maksymowicz A., Vargas G., Vera E., Contreras-Reyes E., Rebolledo S. (2014). Exploring the shallow structure of the San Ramón thrust fault in Santiago, Chile (~ 33.5 S), using active seismic and electric methods. *Solid Earth*, 5(2): 837-849.

Freddi, F., Galasso, C., Cremen, G., Dall'Asta, A., Di Sarno, L., Giaralis, A., Gutiérrez-Urzúa, L.F., Málaga-Chuquitaype, C., Mitoulis, S., Petrone, C., Sextos, A., Sousa, L., Tarbali, K., Tubaldi, E., Wardman, J., Woo, G. (2021). Innovations in Earthquake Risk Reduction for Resilience: Recent Advances and Challenges. *International Journal of Disaster Risk Reduction*, 60: 102267.

Grant D., Fenves G., Whittaker A. (2004). Bidirectional modelling of high-damping rubber bearings. *Journal of Earthquake Engineering*, 8(1):161-185.

INN (2013). *NCh2745: Analysis and design of buildings with seismic isolation* (In Spanish). Instituto Nacional de Normalización.

INN (1996). *NCh433: Earthquake resistant design of buildings* (In Spanish). Instituto Nacional de Normalización.

Kumar M., Whittaker A.S., Constantinou M.C. (2014), An advanced numerical model of elastomeric seismic isolation bearings, *Earthquake Engineering and Structural Dynamics*, 43(13): 1955–1974.

Leonard M. (2010). Earthquake fault scaling: Self-consistent relating of rupture length, width, average displacement, and moment release. *Bulletin of the Seismological Society of America*, 100(5A): 1971-1988.

Liu P., Archuleta R., Hartzell S. (2006). Prediction of Broadband Ground-Motion Time Histories: Hybrid Low / High-Frequency Method with Correlated Random Source Parameters. *Bulletin of the Seismological of America*, 96: 2118–2130.

McKenna F., Fenves G.L., Scott M.H. (2000). Open system for earthquake engineering simulation (OpenSees), University of California, Berkeley.

Ruiz S., Madariaga R. (2018), Historical and recent large megathrust earthquakes in Chile. *Tectonophysics*, 733: 37-56

Schmedes J., Archuleta R., Lavallee D. (2013). A kinematic rupture model generator incorporating spatial interdependency of earthquake source parameters. *Geophysical Journal International*, 192: 1116–1131.

Simpson B., Kakoty P., Ortega M., Hassan W. (2018). *Resilience reconnaissance for hospitals after the 2010 Maule earthquake*, Technical report, Earthquake Engineering Research Institute (EERI), California.